A Comparison of Numerical Simulations and Laboratory Studies of Laser Thrombolysis

E. J. Chapyak and R. P. Godwin

Applied Theoretical and Computational Physics Division
Los Alamos National Laboratory
Los Alamos, New Mexico 87545

S. A. Prahl and H. Shangguan

Oregon Medical Laser Center
Providence St. Vincent Hospital
Portland, Oregon 97225

ABSTRACT

We compare Los Alamos numerical simulations with Oregon Medical Laser Center laser deposition experiments conducted with gelatin thrombus surrogates specifically chosen for relevance to clinical laser thrombolysis. Initial idealized calculations suggest that a surprisingly large fraction of the absorbed laser energy appears as acoustic radiation.[1] We build on these results here by investigating geometrical effects, material property variations, and sources of dissipation including viscosity and plastic flow, as well as acoustic radiation, in an effort to explain flow effects observed in the experiments. In particular, strong jetting is observed in the simulations when the gelatin is given a kinematic viscosity in excess of ~ 1.0 cm^2/s. Jetting is clearly evident in the experiments.

Keywords: laser thrombolysis, bubble dynamics, numerical methods, hydrodynamics, dissipation

1. INTRODUCTION

For the past few years, the Oregon Medical Laser Center (OMLC) has conducted laser energy deposition experiments with gelatin thrombus surrogates.[2] These experiments have generally consisted of gelatin and water in planar contact. A thin layer of gelatin, directly below the water, is impregnated with a dye that mimics the photo absorption characteristic of human thrombus. An optical fiber positioned in the water above the gelatin-water interface delivers laser energy that is transmitted through the intervening water and absorbed in the colored gelatin.

Figure 1 shows a sequence of nominally identical OMLC experiments, each one photographed at a different time. Here, a 577 nm dye laser delivers 50 mJ of energy in approximately 1 μs through an optical fiber, about 0.33 mm in diameter, terminated 1 mm above the gelatin-water interface. The dye layer in the 175 bloom gelatin is 1 mm thick and has an absorption coefficient of 250 cm^{-1}. These experiments are confined within a cuvette of 1 cm by 1 cm square cross section. The gelatin layer in the cuvette is 4 cm thick and is covered with about 2 cm of water, above which is air at atmospheric pressure.

The experimental time sequence shown in Fig. 1 is interesting in several respects. The radius-time behavior of a permanent gas bubble in a uniform unbounded fluid will exhibit approximate symmetry between expansion and collapse. That is, the time from collapse to expansion is approximately equal to the time from expansion to recollapse. The bubbles in Fig. 1 on the water side of the interface do not exhibit such time symmetry. Taking 100 μs as the approximate time to reach maximum expansion after growth initiation, we see that these bubbles persist well beyond 200 μs, to at least 300 μs. The bubble growth in the gelatin cannot be observed directly, although the displacement of the colored layer can be seen. In any event jetting of gelatin into the water is observed from about 300 μs on. The most straightforward interpretation of these data is that the bubble in the gelatin is collapsing faster than the water-side bubble, resulting in the observed jetting.

SPIE Vol. 2970 • 0277-786X/97/$10.00

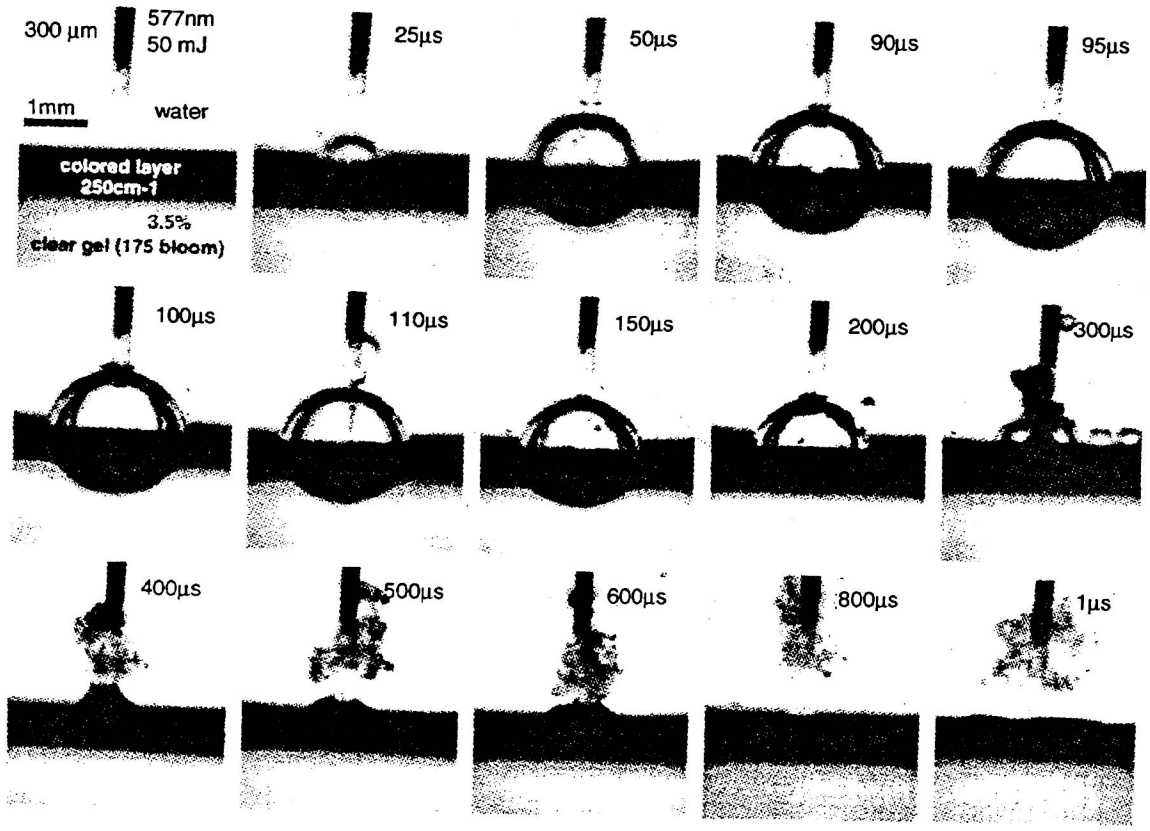

Fig. 1. OMLC laser deposition experimental time sequence.

2. POSSIBLE EXPLANATIONS

Jetting has been observed frequently in studies of bubble dynamics, usually in conjunction with the presence of nearby solid boundaries.[3] Our numerical simulations of experimental-like configurations suggest that the influence of the fiber optic probe and vertical cuvette walls, although significant enough to induce perturbations from unbounded bubble dynamics, cannot by themselves or in concert explain the observed jetting. The proximity of the vertical walls to the bubble may be a contributing cause of the observed time asymmetry, however.

Another potentially fruitful avenue to explore is the impact of differences in material properties between the gelatin and water. Of particular interest in this regard are properties that lead to energy dissipation, which can have an effect on bubble dynamics, as described below. A more dissipative medium generally will result in faster bubble collapse. Thus, if we can argue that gelatin is more dissipative than water, we might be able to explain some of the experimental observations.

We consider three material properties that result in dissipation: acoustic radiation (speed of sound), plastic deformation (material strength) and viscosity.* In order for the gelatin to exhibit more dissipation than water from acoustic radiation, its speed of sound would have to be less than the speed of sound in water. Gelatin sound speeds are generally reported to be very close to that of water and, if anything, one would expect sound speeds in gelatin to be larger than those in water. Gelatin does have some small material strength and can undergo plastic deformation. Typical flow stresses and shear moduli are so

* Strictly speaking, acoustic radiation is not dissipative in the sense of generating entropy. It does remove energy from local bubble dynamics with an effect similar to that caused by true dissipation.

small, however, that any resultant energy dissipation is negligible. We have demonstrated this with computer simulations as well as with back-of-the-envelope estimates. This leaves us with viscosity. Experimental evidence for large gelatin viscosity does exist.[4] In the following, we will focus on viscosity both from a computational and a tutorial viewpoint. Other sources of dissipation are expected to have qualitatively similar effects on bubble dynamics.

3. APPROACH

Our goal is to investigate the behavior of the OMLC experiments qualitatively. We make no effort to simulate exactly experimental conditions and constraints. To do so would add unnecessary complexity and would sacrifice links and comparisons with our previous work. Because the coupling of laser energy into bubble motion under the OMLC experimental conditions is complex, we choose to make extensive use of the test problem described in Ref. 1. We initialize bubble growth from a high pressure, spherical gas bubble of radius 0.00944 cm containing 505 bars of $\gamma = 1.4$ ideal gas at 5100 K. In incompressible, unbounded water, this bubble expands to 0.1 cm radius, about the maximum size of the OMLC bubbles. We note, however that the OMLC bubbles contain condensable vapor rather than permanent gas. These initial conditions and geometry will be employed in all the numerical simulations described below. In order to investigate viscous effects, we implemented a Newtonian viscosity model into our Eulerian finite difference code, MESA-2D.[1] This work was done by Patrick J. Blewett. The new coding was tested on Stokes' first problem,[5] boundary layer growth in a semi-infinite fluid generated by an impulsively accelerated flat plate. Code results reproduced the analytical solution for this problem to within a few tenths of a percent.

4. QUALITATIVE EFFECT OF VISCOSITY

The Rayleigh-Plesset (R-P) Equation, which describes the growth of spherical gas cavities surrounded by an incompressible, unbounded liquid, is

$$\rho\left(R\ddot{R}+[3/2]\dot{R}^2\right)=P_g-P-2\sigma/R-4\mu\dot{R}/R, \tag{1}$$

where R is the cavity radius, the dot denotes differentiation with respect to time, P_g the gas pressure inside the cavity, P the liquid pressure at infinity, σ the liquid-cavity surface tension, and μ the liquid's viscosity coefficient. If we multiply Eq. 1 by $\dot{V}$, the time derivative of the cavity volume, and integrate once, an energy conservation equation is obtained. If P_g is a function of cavity volume only (We will always assume an adiabatic relationship, $P_g V^{\gamma}$ = constant.), and surface tension is neglected, this energy equation can be expressed as

$$\Delta\left(2\pi\rho R^3\dot{R}^2+P_gV/(\gamma-1)\right)+D=-P\Delta V, \tag{2}$$

where $\Delta F = F(2) - F(1)$ for any function F, and

$$D=4\mu\int_{V(1)}^{V(2)}\left(\dot{R}/R\right)dV. \tag{3}$$

Note that D is positive definite because $\dot{R}\le 0$ when $dV\le 0$ and conversely. Equation 2 states that the change in the liquid's kinetic energy plus the change in the internal energy of the gas plus the dissipated energy between two states is equal to the work done on the bubble-liquid system by the external environment.

Take state 1 to be the (initial) point of maximum compression. Then $\dot{R}(1)=0$ and Eq. 2 can be written as

$$2\pi\rho R^3(2)\dot{R}^2(2)+\frac{P_g(2)V(2)-P_g(1)V(1)}{\gamma-1}+D=-P[V(2)-V(1)]. \tag{4}$$

Consider two cases, $D\equiv 0$, and $D>0$. Let $R(2)$ be identical for both cases. By definition $R(1)$ is also the same for both cases. Equation 4 implies that

$$\dot{R}^2(2)_{D=0}=\dot{R}^2(2)_{D>0}+\left(D/2\pi\rho R^3(2)\right), \text{ or } \dot{R}^2(2)_{D=0}>\dot{R}^2(2)_{D>0}. \tag{5}$$

By selecting state 2 in Eq. 4 to be the point of maximum expansion, one can also show that

$$V_{D=0}>V_{D>0} \text{ (at maximum expansion)}. \tag{6}$$

Finally, we consider Eq. 1 at the point of maximum expansion, and Eq. 5, to conclude that

$$\left|\ddot{R}_{D>0}\right|>\left|\ddot{R}_{D=0}\right| \text{ (at maximum expansion)}. \tag{7}$$

Equations 5, 6, and 7 taken together strongly suggest that the radius-time curve for a bubble in a fluid with dissipation will lie wholly below the corresponding curve for a fluid without dissipation, assuming that both initial states are the same maximum compression state.

This behavior is indeed confirmed by numerical simulation. Figure 2 compares the R-P radius-time prediction for a zero viscosity and surface tension incompressible fluid (water) to numerical simulations first with compressibility but no viscosity and then with both compressibility and viscosity. In all cases the initial conditions are as described in Section 3. The equation of state for water in the simulations was the SESAME[6] 7152 table, which is based on NIST data.[7] We note from Fig. 2 that as additional sources of dissipation are considered, namely acoustic radiation and then acoustic radiation plus viscosity, the radius-time curve drops farther below the R-P (nondissipative) result. The amount of energy depleted from the bubble motion at the point of maximum expansion can be determined easily from volume differences. Acoustic radiation alone accounts for about a 16% energy deficit; acoustic radiation plus a kinematic viscosity ($\nu = \mu / \rho$) of 1.0 cm^2/s results in a 25% energy deficit. The available energy, or energy scale, is essentially the pressure at infinity multiplied by the maximum bubble volume. We determined in Ref. 1 that the energy channeled into acoustic radiation was consistent with analytical estimates for this problem. In the next section, we derive an energy estimate for viscous dissipation.

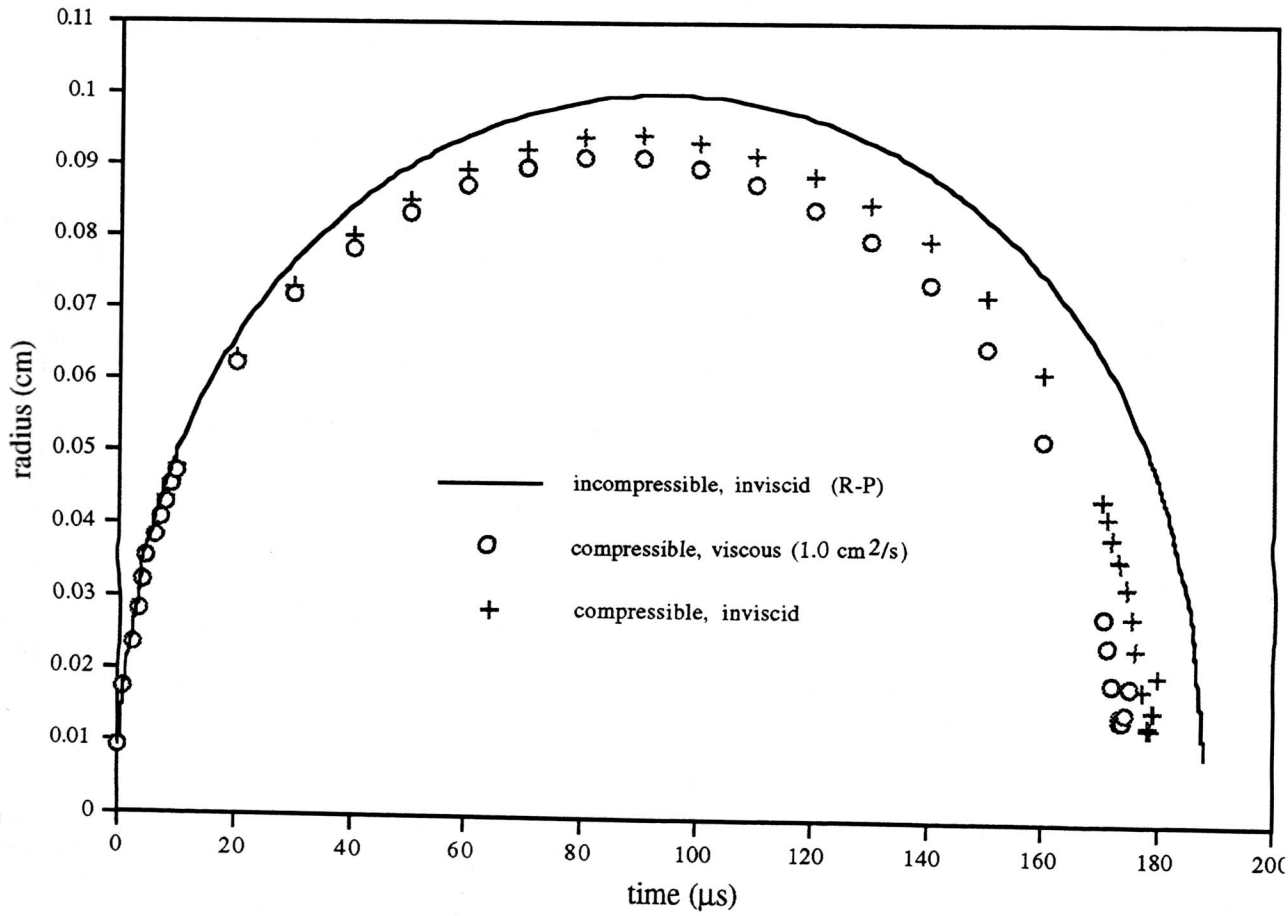

Fig. 2. Bubble radius-time comparisons for various sources of dissipation.

5. ENERGY DISSIPATION ESTIMATE FOR VISCOSITY

We can approximately evaluate D from its expression above, using the R-P zero viscosity radius-time solution. A first integral of Eq. 1, neglecting both viscosity and surface tension, can be obtained easily:

$$\dot{R}^2 = \frac{2}{3}\frac{P}{\rho}\left(\frac{V_m}{V}-1\right)+\frac{2}{3}\frac{P_m}{\rho(\gamma-1)}\frac{V_m}{V}\left[1-\left(\frac{V_m}{V}\right)^{\gamma-1}\right], \tag{8}$$

where the subscript m refers to the initial point of maximum compression.. Since

$$\dot{R}^2 \le \frac{2}{3}\frac{P_m}{\rho(\gamma-1)}\frac{V_m}{V}\left[1-\left(\frac{V_m}{V}\right)^{\gamma-1}\right], \tag{9}$$

D, from initial compression to full expansion, can be bounded by Eq. 3 with $\dot{R}$ specified by Eq. 9. This leads to

$$D \le \frac{4\mu V_m}{R_m}\sqrt{\frac{2P_m}{3\rho(\gamma-1)}}\int_{V_m/V_o}^{1}\frac{\sqrt{1-u^{\gamma-1}}}{u^{7/6}}du \le \frac{4\mu V_m}{R_m}\sqrt{\frac{2P_m}{3\rho(\gamma-1)}}\int_{V_m/V_o}^{1}\frac{du}{u^{7/6}}, \tag{10}$$

where the subscript o denotes the state of maximum expansion. Evaluation of Eq. 10 gives

$$\frac{D}{PV_o} \le \frac{24\nu}{R_m}\sqrt{\frac{2\rho(\gamma-1)R_o}{3P_mR_m}}. \tag{11}$$

For the problem presented in Fig. 2, Eq. 11 reduces to $D/PV_o \le 0.19\nu(\mathrm{cm}^2/\mathrm{s})$, which can be compared to the observation from Fig. 2 that about 10% of the available energy is dissipated by viscous effects for $\nu = 1.0$ cm^2/s.

6. NUMERICAL SIMULATIONS WITH DISSIPATIVE GELATIN

We next describe numerical simulations of bubble dynamics in a gelatin-water system similar to the OMLC experimental configuration. The initial state of the gas bubble is as described in Section 3, with the center of the gas sphere located at the water-gelatin interface. Both water and gelatin are described by the SESAME 7152 equation-of-state, but the gelatin is given a kinematic viscosity of 5.0 cm^2/s, while the water is treated as inviscid. A solid cylinder, simulating the optical fiber, is also included. The boundaries are all 2.53 cm from the center of the gas sphere, with rigid boundaries being used on the radial boundary and the gelatin-side axial boundary. A transmissive (zero gradient) boundary is used on the water-side axial boundary. This boundary configuration has been shown to closely approximate unbounded fluid behavior as far as the bubble dynamics are concerned.

Figure 3 shows the expansion phase material interfaces for this problem. Gelatin occupies the left half-space and water occupies the right half-space with the initial sphere of gas centered at r = z = 0. Water-gelatin, gas-water, gas-gelatin, and water-optical fiber interfaces are shown. (The "blemishes" in Fig. 3 are artifacts of the interface reconstruction algorithm in MESA-2D.) Note that the gas bubble expands more rapidly into the water than into the gelatin. Also note that, at the last time included in Fig. 3, 80 μs, the gelatin-side bubble has stopped its expansion, while the water-side bubble is still expanding. This behavior is consistent with the single-fluid results discussed in Section 4. Figure 4 is a continuation in time of Fig. 3, when the bubble is collapsing. Here, the gelatin-side collapse continues to lead the water-side collapse. In addition, a perturbation originates near the gelatin-water interface and collapses on axis ahead of the axial collapse of either the gelatin or water sides. After converging on axis, this perturbation generates jetting in both axial directions. The post collapse state of the bubble is shown in Fig. 5 at 178 μs along with velocity vectors. The axial jets have penetrated the remnant bubble to leave a toroidal bubble structure. Jet velocities greater than 10 m/s are apparent.

7. CONCLUSIONS

Dissipative mechanisms in gelatin have been investigated as possible explanations for the jetting observed in OMLC laser deposition experiments. Viscosity appears to be a more likely source of this dissipation than either acoustic radiation (compressibility) or plastic flow. We have shown that jetting can be produced in numerical simulations of Laser Thrombolysis-related bubble dynamics when the gelatin is assumed to be significantly more viscous than water. However, actual ejection of gelatin into the water, as seen in the experiments, is not evident in these simulations. Preliminary work indicates that the relatively close proximity of vertical cuvette walls to the laser-induced bubble may help explain observed time asymmetries in the bubble motion.

8. ACKNOWLEDGMENTS

This work was supported in part by a Cooperative Research and Development Agreement (CRADA) between Los Alamos National Laboratory (Department of Energy), Oregon Medical Laser Center, and Palomar Medical Technologies. The first two authors thank Patrick J. Blewett, of Los Alamos, for implementing and testing a Newtonian viscosity model in MESAS-2D.

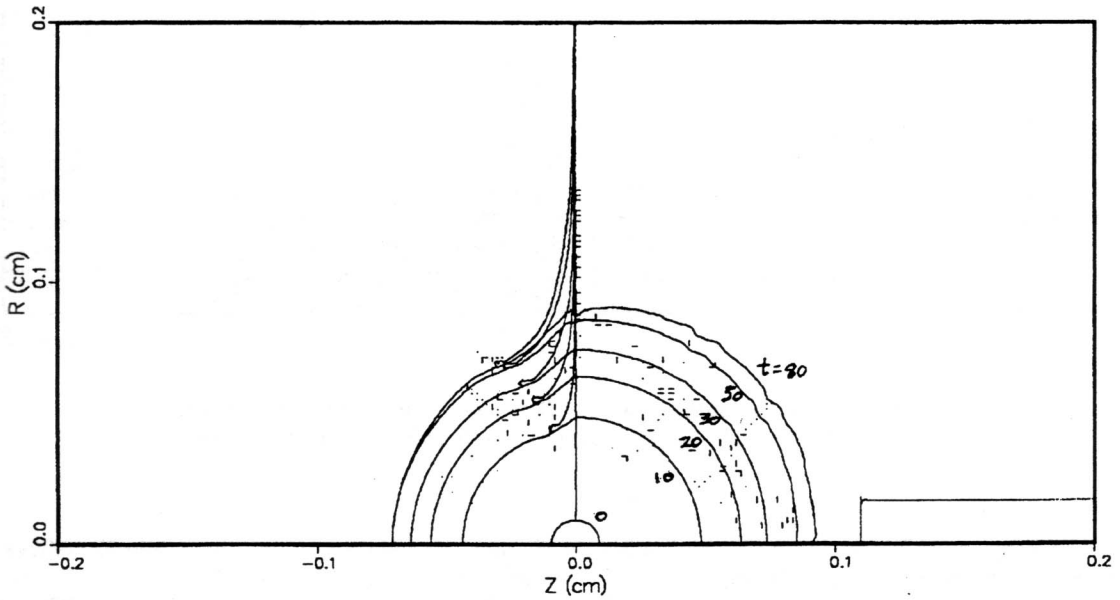

Fig. 3. Material interface time sequence during bubble expansion.
(Times are in μs. Water is on the right, gelatin is on the left.)

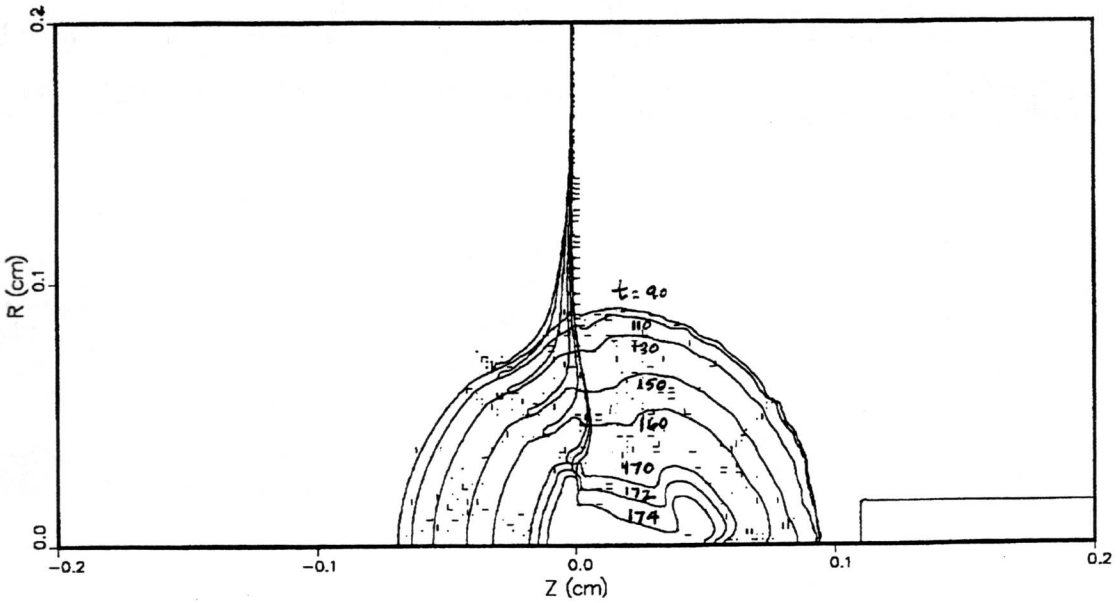

Fig. 4. Material interface time sequence during bubble contraction.

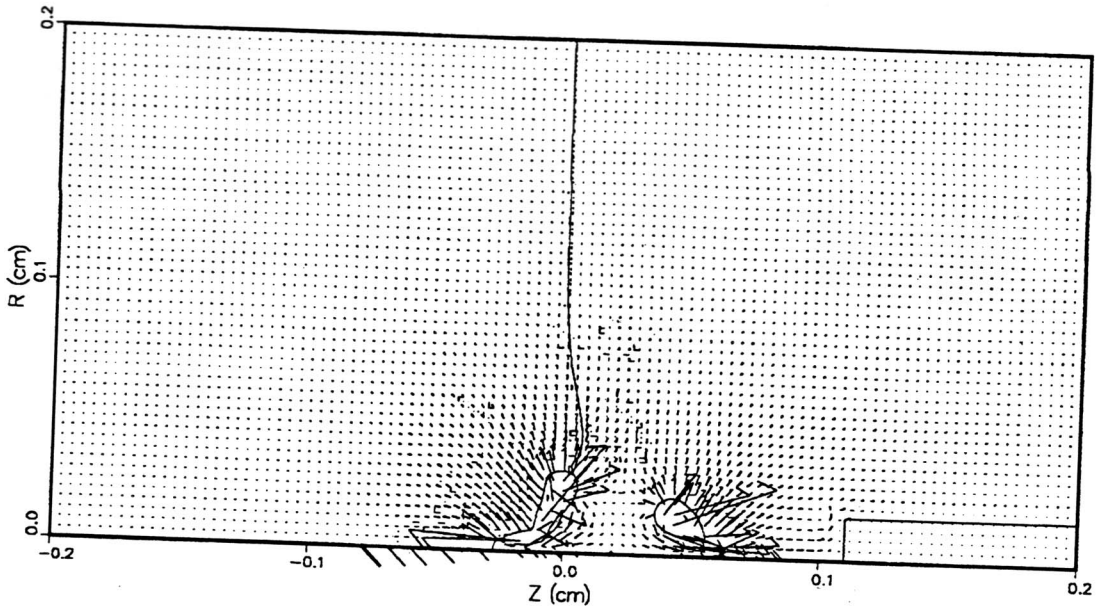

Fig. 5. Material interface plot at 178 μs, with velocity vectors indicated.
Note the toroidal gas bubble shapes and the axial jets along the z-axis.

8. REFERENCES

1. E. J. Chapyak and R. P. Godwin, "Numerical Studies of Bubble Dynamics in Laser Thrombolysis," *Lasers in Surgery: Advanced Characterization, Therapeutics, and Systems VI, Proc. SPIE*, **2671**, 84, 1996.

2. U. S. Sathyam, A. Shearin, E. A. Chasteney, and S. A. Prahl, "Threshold and Ablation Efficiency Studies of Microsecond Ablation of Gelatin Under Water," *Lasers in Surgery and Medicine*, 19, 397, 1996.

3. M. S. Plesset and A. Prosperetti, "Bubble Dynamics and Cavitation," *Ann. Rev. Fluid Mech.*, **9**, 145, 1977.

4. J. K. Dienes, P. L. Coleman, M. Intaglietta, and J. E. Welch, "The Response of Gelatin to High Speed Impact," Systems, Science and Software report SSS-R-73-1891, 1973.

5. H. Schlichting, *Boundary-Layer Theory*, p.90, McGraw-Hill Book Co., 1979.

6. K. S. Holian, "T-4 Handbook of Material Properties Data Bases," Los Alamos National Laboratory report LA-10160-MS, 1984.

7. L. Haar and J. S. Gallagher, "A Thermodynamic Surface for Water: The Formulation and Computer Programs," National Bureau of Standards internal report 81-2253, 1981.